arXiv:1506.05434v1 [hep-ph] 17 Jun 2015

Coexistence of Multiple Phases in Magnetized Quark Matter with Vector Repulsion

Robson Z. Denke[1, 2, *] and Marcus Benghi Pinto[1, †]

[1] *Departamento de Física, Universidade Federal de Santa Catarina, 88040-900 Florianópolis, Santa Catarina, Brazil*
[2] *Departamento de Física, Fundação Universidade Regional de Blumenau, 89012-900 Blumenau, Santa Catarina, Brazil*

We explore the phase structure of dense magnetized quark matter when a repulsive vector interaction, parametrized by G_V, is present. Our results show that for a given magnetic field intensity (B) one may find a value of G_V for which quark matter may coexist at three different baryonic density values leading to the appearance of two triple points in the phase diagram which have not been observed before. Another novel result is that at high pressure and low temperature we observe a first order transition which presents a negative slope in the $P-T$ that is reminiscent of the solid-liquid transition line observed within the water phase diagram. These unusual patterns occur for G_V and B values which lie within the range presently considered in many investigations related to the study of magnetars.

PACS numbers: 11.10.Wx, 26.60.Kp,21.65.Qr, 25.75.Nq

I. INTRODUCTION

Strongly interacting magnetized matter may be produced in non central relativistic heavy ion collisions [1] and may also be present in magnetars [2] reaching up about to $\sim 10^{19}\,G$ and $\sim 10^{18}\,G$ in each of these two physical situations. As far as heavy ion-collisions are concerned the presence of a strong magnetic field most certainly plays a role despite the fact that, in principle, the field intensity should decrease very rapidly lasting for about 1-2 fm/c only [1]. The possibility that this short time interval may [3] or may not [4] be affected by conductivity remains under dispute.

A striking property expected to occur in such extreme conditions is the so called Magnetic Catalysis (MC) phenomenon [5], which implies that the order parameter for the chiral transition represented by the quark-antiquark condensate rises as the field becomes more intense (see Ref. [6] for a review). It is then natural to ask how the expected quantum chromodynamics (QCD) transitions are affected by the presence of intense magnetic fields, a question which has been addressed in many recent works (see Refs. [7] for an updated discussion). To summarize the main results obtained in these investigations let us start by recalling that at finite temperatures and vanishing chemical potential both, model approximations [8–11] and lattice QCD (LQCD) evaluations [12, 13] agree that a cross over, which is predicted to occur in the the absence of magnetic fields [14], persists when strong magnetic fields are present. However, a source of disagreement between recent LQCD evaluations [13] and model predictions regards the behavior of the pseudocritical temperature ($T_{\rm pc}$), at which the cross over takes place, as a function of the magnetic field intensity. The LQCD simulations of Ref. [13], performed with $2+1$ quark flavors and physical pion mass values, predict that $T_{\rm pc}$ should decrease with B while early model evaluations predict an increase (see Ref. [9] and references therein). This problem has been recently addressed by different groups [15] which basically agree that the different results stem from the fact that most effective models miss back reaction effects (the indirect interaction of gluons and B) as well as the QCD asymptotic freedom phenomenon. On the other hand, LQCD results are currently unavailable at high densities and low temperatures so that one has to rely in model approximations [9–11] which predict that the first order chiral transition takes place at a coexistence chemical potential value which is lower than the one observed for the case of unmagnetized matter leading to the phenomenon called Inverse Magnetic Catalysis (IMC) [16] (see Ref. [17] for a physically intuitive discussion of the IMC phenomenon). Further investigations performed with the Nambu–Jona-Lasinio model (NJL) have been carried out to locate the critical end point (CP) as well as the coexistent chemical potentials associated with the first order chiral transition [9, 11]. The results suggest that the size of first order transition line increases as the field becomes stronger affecting the position of the (second order) CP where the first order transition line terminates. At the same time, the size and location of the coexistence region in the presence of a magnetic field appears to oscillate around the $B=0$ values [18]. Together, all these effects have interesting consequences for quantities which depend on the details of the coexistence region such as the surface tension and may have consequences for studies related to the properties of magnetized compact stellar objects [19]. The motivation for the present investigation stems from an early work by Ebert and collaborators [20] who recognized that

*Electronic address: r.denke@posgrad.ufsc.br
†Electronic address: marcus.benghi@ufsc.br

the MC phenomenon, associated to the filling of Landau levels, could lead to more exotic phase transition patterns as a consequence of the induced magnetic oscillations. To confirm this assumption these authors have considered a wide range of the (scalar) coupling values for the two flavor NJL model at vanishing temperatures and, as expected, have observed unusual phase structures as a function of the chemical potential such as an infinite number of massless chirally symmetric phases, a cascade of massive phases with broken chiral invariance among other features. More recently, this seminal study has been extended by a more systematic, and numerically accurate analysis with two and three flavors in Refs. [21] and [22] respectively. The results confirm that for certain model parametrizations one is able to observe more than one first order phase transition, which is signaled when the thermodynamical potential develops two degenerate minima at different values of the coexistence chemical potential [1]. It is important to remark that, in general, *weak* first order transitions can be easily missed in a numerical evaluation due to the fact that the two degenerate minima appear almost at the same location being separated by a tiny potential barrier so that their study requires extra care. Physically, this corresponds to a situation where two different (but almost identical) densities coexist at the same chemical potential, temperature and pressure. Here, one of our goals is to extend the investigation of these cascades of first order phase transitions, observed in Refs. [20–22], when *hot* magnetized quark matter is subject to the presence of a repulsive vector channel parametrized by G_V. This type of interaction provides a saturation mechanism similar to those found in effective nuclear models [24] and is known to be important for an accurate description of quark matter at high baryonic densities [25]. As we have verified in a previous work [18], the repulsive vector coupling modifies the magnetic effects mainly at lower temperatures and plays an opposite role compared to B in the QCD phase diagram. As a matter of fact, the increase of the magnetic field shifts the first order transition to lower values of the coexistence chemical potential while a nonzero vector repulsion produces the reverse effect. This feature has also been recently verified within the three flavor case [26] in the analysis of compact stellar objects. Here, we shall see that the presence of a vector repulsion allows for further interesting possibilities associated with the chiral first order transition due to the fact that this term can stabilize intermediary density magnetic phases. Being carried out at finite temperatures the present investigation also allows for a more complete description of the coexistence region and makes it possible to better understand the physical nature of the associated phase transitions. As a first novelty we show that within a cascade of the transitions the one which takes place at the highest pressure value seems to be reminiscent of the "solid-liquid" type of transition displayed by the phase diagram of water while the others are of the usual "liquid-gas" type (commonly observed within QCD effective theories). Motivated by the fact that the Lennard-Jones potential, which describes water, also has a repulsive part we have scanned over the G_V values to search for any eventual triple point in the phase diagram of magnetized quark matter since this situation cannot be completely ruled out in the scenario considered here. The reason is that the presence of a magnetic field induces the free energy to develop multiple minima while the repulsive interaction favors stability so that eventually three (instead of the usual two) minima could be globally degenerate leading to the coexistence of three phases. As we shall demonstrate the numerical results have confirmed our expectations so that for very particular, but yet realistic, parameter values the phase diagram of strongly interacting magnetized quark matter may indeed display triple points.

The work is organized as follows. In the next section we present the free energy in the presence of a repulsive vector channel for the magnetized NJL model within the mean field approximation (MFA) framework. In Sec. III we discuss how a cascade of the usual type of first order phase transitions, with two degenerate minima, takes place at finite temperatures. In the same section we extend the analysis to the finite temperature domain in order to draw the phase diagrams in the $T-\mu$, $T-\rho_B$ and $P-T$ planes. Section IV is devoted to the study of unusual first order phase transitions where the free energy develops more than two degenerate minima allowing for the existence of triple points. Our conclusions and final remarks are presented in Sec. V.

II. NJL MAGNETIZED FREE ENERGY WITH A REPULSIVE VECTOR INTERACTION

The QCD interaction between quarks can be effectively described by the well-known NJL theory [27] which reproduces, at lower energies, the main features of chiral symmetry breaking. In the usual two flavor version the same coupling constant, G_S, sets the interaction strength in both the scalar and pseudo-scalar channels. However, in finite density investigations the model produces more realistic results if an additional repulsive vector channel, parametrized by G_V, is introduced. In this case, the corresponding Lagrangian density [25, 28] can be written as

$$\mathscr{L} = \bar{\psi}(i\gamma_\mu\partial^\mu - m)\psi + G_S[(\bar{\psi}\psi)^2 + (\bar{\psi}i\gamma_5\vec{\tau}\psi)^2] - G_V(\bar{\psi}\gamma^\mu\psi)^2, \tag{2.1}$$

[1] This fact has also been recently observed to arise within another effective four fermion theory described by the $2+1$ d Gross-Neveu model [23].

where $m = m_u \simeq m_d$ is the bare quark mass. In order to derive the thermodynamical potential within the MFA the quadratic interaction terms appearing in the above Lagrangian are linearized by the introduction of the mean fields expressed in terms of the scalar condensate, $\phi = \langle\bar{\psi}\psi\rangle$, and the quark number density, $\rho = \langle\psi^+\psi\rangle$

$$(\bar{\psi}\psi)^2 \simeq 2\phi\bar{\psi}\psi - \phi^2 \quad \text{and} \quad (\bar{\psi}\gamma^0\psi)^2 \simeq 2\rho\psi^+\psi - \rho^2 \ , \tag{2.2}$$

where quadratic terms in the fluctuations have been neglected while the pseudo-scalar term does not contribute at this level. Then, in the case of symmetric quark matter ($\mu = \mu_u = \mu_d$) the theory is described by

$$\mathscr{L} = \bar{\psi}(i\gamma_\mu\partial^\mu - M + \tilde{\mu}\gamma^0)\psi - \frac{(M-m)^2}{4G_S} + \frac{(\mu-\tilde{\mu})^2}{4G_V} \ , \tag{2.3}$$

where the effective quark mass, M, and the effective chemical potential, $\tilde{\mu}$, are determined upon applying the corresponding minimization conditions, $\delta\Omega/\delta M = 0$ and $\delta\Omega/\delta\tilde{\mu} = 0$. Integrating over the fermionic fields yields the thermodynamical potential

$$\Omega = \frac{(M-m)^2}{4G_S} - \frac{(\mu-\tilde{\mu})^2}{4G_V} + \frac{i}{2}\mathrm{tr}\int\frac{d^4p}{(2\pi)^4}\ln[-p^2 + M^2] \ . \tag{2.4}$$

One can then include the effects of a static magnetic field and a thermal bath to this dense quark matter system by applying the following replacements [29] to Eq. (2.4):

$$p_0 \to i(\omega_\nu - i\mu) \ ,$$

$$p^2 \to p_z^2 + (2n + 1 - s)|q_f|B \quad , \text{ with } \ s = \pm 1 \ , \ n = 0, 1, 2... \ ,$$

$$\int_{-\infty}^{+\infty}\frac{d^4p}{(2\pi)^4} \to i\frac{T|q_f|B}{2\pi}\sum_{\nu=-\infty}^{\infty}\sum_{n=0}^{\infty}\int_{-\infty}^{+\infty}\frac{dp_z}{2\pi} \ ,$$

where $\omega_\nu = (2\nu + 1)\pi T$ ($\nu = 0, \pm1, \pm2...$) represents the Matsubara frequencies for fermions. The Landau levels are labelled by n while the absolute values of quark electric charges $|q_f|$ are $|q_u| = 2e/3$ and $|q_d| = e/3$ with $e = 1/\sqrt{137}$ representing the electron charge [2]. Then, following Ref. [30] we can write the thermodynamical potential as

$$\Omega = \frac{(M-m)^2}{4G_S} - \frac{(\mu-\tilde{\mu})^2}{4G_V} + \Omega_{vac} + \Omega_{mag} + \Omega_{med} \ , \tag{2.5}$$

where the vacuum contribution reads

$$\Omega_{vac} = -2N_cN_f\int\frac{d^3\mathbf{p}}{(2\pi)^3}\sqrt{p^2 + M^2} \ , \tag{2.6}$$

and, as usual, can be regularized by a non-covariant sharp cut-off, Λ, yielding

$$\Omega_{vac} = \frac{N_cN_f}{8\pi^2}\left\{M^4\ln\left[\frac{(\Lambda + \epsilon_\Lambda)}{M}\right] - \epsilon_\Lambda\Lambda[\Lambda^2 + {\epsilon_\Lambda}^2]\right\} \ , \tag{2.7}$$

where ϵ_Λ represents the energy $\sqrt{\Lambda^2 + M^2}$ at the cutoff momentum value Λ. We remark that in Refs. [31, 32] the authors choose a smooth cut off to avoid unphysical oscillations, which appear when the pairing interaction is included

[2] Our results are expressed in Gaussian natural units where $1\,\mathrm{MeV}^2 = 1.44 \times 10^{13}\,G$.

because the sharp cut off limits the allowed momenta. In the present work, no superconducting phase (that would require the pairing gap equation to be solved) is used and hence we do not face the problem of unphysical solutions. The magnetic contribution of the thermodynamical potential is given by

$$\Omega_{mag} = -\sum_{f=u}^{d} \frac{N_c(|q_f|B)^2}{2\pi^2}\left\{\zeta'[-1,x_f] - \frac{1}{2}(x_f^2 - x_f)\ln x_f + \frac{x_f^2}{4}\right\}, \tag{2.8}$$

whre we have used the definition $x_f = M^2/(2|q_f|B)$ and the derivative of the Riemann-Hurwitz zeta function $\zeta'(-1,x_f) = d\zeta(z,x_f)/dz|_{z=-1}$ (see the appendix of Ref. [30] for detailed steps). Finally, the term Ω_{med} represents the in-medium contribution

$$\Omega_{med} = -\frac{N_c}{2\pi}\sum_{f=u}^{d}\sum_{k=0}^{\infty}\alpha_k(|q_f|B)\int_{-\infty}^{\infty}\frac{dp_z}{2\pi}\left\{T\ln\left[1+e^{-(E_p+\tilde{\mu})/T}\right] + T\ln\left[1+e^{-(E_p-\tilde{\mu})/T}\right]\right\} \ , \tag{2.9}$$

where $\alpha_k = 2-\delta_{k0}$ and $E_p = \sqrt{p_z^2+2k|q_f|B+M^2}$. A similar expression for the magnetized thermodynamical potential at $G_V = 0$ was originally obtained in Ref. [33] where Schwinger's proper time approach has been used. Solving $\delta\Omega/\delta M = 0$ and $\delta\Omega/\delta\tilde{\mu} = 0$ we get the following coupled self consistent equations

$$M = m - 2G_S\phi \ , \tag{2.10}$$

and

$$\tilde{\mu} = \mu - 2G_V\rho \ , \tag{2.11}$$

Note also that, in principle, one should have two coupled gap equations for the two distinct flavors: $M_u = m_u - 2G_S(\langle\bar{u}u\rangle + \langle\bar{d}d\rangle)$ and $M_d = m_d - 2G_S(\langle\bar{d}d\rangle + \langle\bar{u}u\rangle)$ where $\langle\bar{u}u\rangle$ and $\langle\bar{d}d\rangle$ represent the quark condensates which differ, due to the different electric charges. However, in the two flavor case, the different condensates contribute to M_u and M_d in a symmetric way and since $m_u = m_d = m$ one has $M_u = M_d = M$. The quantities $\phi = \phi_{vac} + \phi_{mag} + \phi_{med}$ and ρ appearing in Eqs. (2.10) and (2.11) are given by

$$\phi_{vac} = -\frac{MN_cN_f}{2\pi^2}\left\{\Lambda\epsilon_\Lambda - \frac{M^2}{2}\ln\left[\frac{(\Lambda+\epsilon_\Lambda)^2}{M^2}\right]\right\} \ , \tag{2.12}$$

$$\phi_{mag} = -\frac{MN_c}{2\pi^2}\sum_{f=u}^{d}|q_f|B\left[\ln\Gamma(x_f) - \frac{1}{2}\ln(2\pi) + x_f - \frac{1}{2}(2x_f-1)\ln(x_f)\right] \ , \tag{2.13}$$

$$\phi_{med} = \frac{MN_c}{2\pi}\sum_{f=u}^{d}\sum_{k=0}^{\infty}\alpha_k(|q_f|B)\int_{-\infty}^{\infty}\frac{dp_z}{2\pi}\frac{1}{E_p}\left[n_p(\tilde{\mu},T) + \bar{n}_p(\tilde{\mu},T)\right] \ , \tag{2.14}$$

and

$$\rho = \frac{N_c}{2\pi}\sum_{f=u}^{d}\sum_{k=0}^{\infty}\alpha_k(|q_f|B)\int_{-\infty}^{\infty}\frac{dp_z}{2\pi}\left[n_p(\tilde{\mu},T) - \bar{n}_p(\tilde{\mu},T)\right] \ , \tag{2.15}$$

where

$$n_p(\tilde{\mu},T) = \frac{1}{1+e^{(E_p-\tilde{\mu})/T}} \ \text{ and } \ \bar{n}_p(\tilde{\mu},T) = \frac{1}{1+e^{(E_p+\tilde{\mu})/T}} \, , \tag{2.16}$$

represent, respectively, the Fermi occupation number for quarks and antiquarks.

At $T = 0$ the relevant in-medium terms appearing in Ω, M and $\tilde{\mu}$ can be written as

$$\Omega_{med} = -\frac{N_c}{4\pi^2}\sum_{f=u}^{d}\sum_{k=0}^{k_{f,max}}\alpha_k|q_f|B\left\{\tilde{\mu}k_F(k,B) - s_f(k,B)^2\ln\left[\frac{\tilde{\mu}+k_F(k,B)}{s_f(k,B)}\right]\right\} \ , \tag{2.17}$$

$$\phi_{med} = \sum_{f=u}^{d} \sum_{k=0}^{k_{f,max}} \alpha_k \frac{M N_c(|q_f|B)}{2\pi^2} \ln\left[\frac{\tilde{\mu} + k_F(k,B)}{s_f(k,B)}\right] , \tag{2.18}$$

and

$$\rho = \sum_{f=u}^{d} \sum_{k=0}^{k_{f,max}} \alpha_k \frac{|q_f|BN_c}{2\pi^2} k_F(k,B) , \tag{2.19}$$

where $k_F(k,B)$ represents the Fermi momentum, $k_F = \sqrt{\tilde{\mu}^2 - s_f(k,B)^2}$, and $s_f(k,B) = \sqrt{M^2 + 2|q_f|kB}$. The upper Landau level (or the nearest integer) is defined by

$$k_{f,max} = \left\lfloor \frac{\tilde{\mu}^2 - M^2}{2|q_f|B} \right\rfloor . \tag{2.20}$$

To obtain numerical results we must now fix the model parameters and, as usual, the cut-off value together the other parameters G_S, m are chosen to reproduce the phenomenological values [28] for the pion mass ($m_\pi \simeq 140\,\mathrm{MeV}$), the pion decay constant ($f_\pi \simeq 93\,\mathrm{MeV}$) and the quark condensate ($\langle\bar{\psi}\psi\rangle^{1/3} \simeq 250\,\mathrm{MeV}$). Here, we consider the set $\Lambda = 590\,\mathrm{MeV}$, $G_S\Lambda^2 = 2.435$ and $m = 6.0\,\mathrm{MeV}$.

Fixing G_V poses and additional problem since this quantity should be fixed using the ρ meson mass which, in general, happens to be higher than the maximum energy scale set by Λ. At present, the vector term coupling G_V cannot be determined from experiments and lattice QCD simulations (LQCD) but eventually, the combination of neutron star observations and the energy scan of the phase-transition signals at FAIR/NICA may provide us some hints on its precise numerical value. Therefore, at the present stage the vector coupling G_V is usually taken to be a free parameter whose accepted values lie within the range $0.25\,G_S - 0.5\,G_S$ [34–36]. It is worth to point out that the explicit use of G_V within the NJL model can be avoided provided that the evaluations be performed beyond the large-N_c (or MFA) level. In this case two loop (exchange like) terms bring finite N_c corrections to the pressure such as $(G_S/N_c)\rho^2$ so that the same type of physics can be observed with one less parameter [37].

III. CASCADE OF FIRST ORDER CHIRAL TRANSITIONS WITH TWO COEXISTING DENSITIES

Within the usual first order transition scenario the free energy develops a pair of degenerate global minima defining two distinct values for the effective quark masses as well as for the quark number density. Usually, when $B = 0$, only one first order chiral transition takes place so that, for a given temperature, a unique value for the coexistence chemical potential exists. However, as already emphasized, the presence of a magnetic field causes an oscillatory behavior which may induce more exotic patterns like the appearance of a cascade of first order transitions such as the ones studied in Refs. [20–22] where only the case of vanishing temperatures, in the absence of repulsion, has been considered. One of the main outcomes of these applications is that, for some phenomenologically acceptable parametrizations, several transitions are needed to move from the vacuum phase to the (approximately) chirally symmetric phase. More recently, Allen, Pagura and Scoccola [38] have observed a similar situation when considering a a generalized version of the two flavor NJL model, which includes a G_V term, but again at vanishing temperatures. In this section we will extend the investigation performed at $G_V \neq 0$ to the finite temperature case to gain extra insight on the effects of B and G_V by exploring the phase diagram in planes such as $T - \mu$, $T - \rho_B$, and $P - T$. This exercise will allow us not only to review some of the main aspects related to the appearance of a cascade of first order phase transitions as the ones studied in Refs. [20–22, 38] but also to explore more realistic finite temperature situations.

Let us first recall that, within this model, the order parameter associated with the chiral transition is $(\langle\bar{u}u\rangle + \langle\bar{d}d\rangle)/2$ which, in our case, is directly related to the effective mass as Eq. (2.10) indicates. Therefore, it is instructive to analyze the effects of B and G_V over M since this quantity also determines the behavior of the associated EoS. The left panel of Fig. 1, which was originally obtained in Ref. [18], displays the effective quark mass, at $T = 0$, as a function of μ for $G_V = 0.2\,G_S$ and different values of the magnetic field. The figure indicates that, in the vacuum, the value of M tends to increase with B which is in accordance with the magnetic catalysis effect [5]. Also, due to the filling of Landau levels, one observes the typical de Haas-van Alphen oscillations which are more pronounced for small values of B. Only the segments of the curves where $dM/d\mu < 0$ correspond to energetically favored gap equation solutions and in the present case ($G_V = 0.2\,G_S$) we observe that for $eB = 5\,m_\pi^2$ and $eB = 8\,m_\pi^2$ some of these solutions are stable leading to intermediate transitions. For example, at $eB = 5\,m_\pi^2$ one sees a first transition at $\mu = 388.55\,\mathrm{MeV}$ when the mass jumps from $409\,\mathrm{MeV}$ to $313\,\mathrm{MeV}$. This is followed by another transition from $M = 312.6\,\mathrm{MeV}$ to

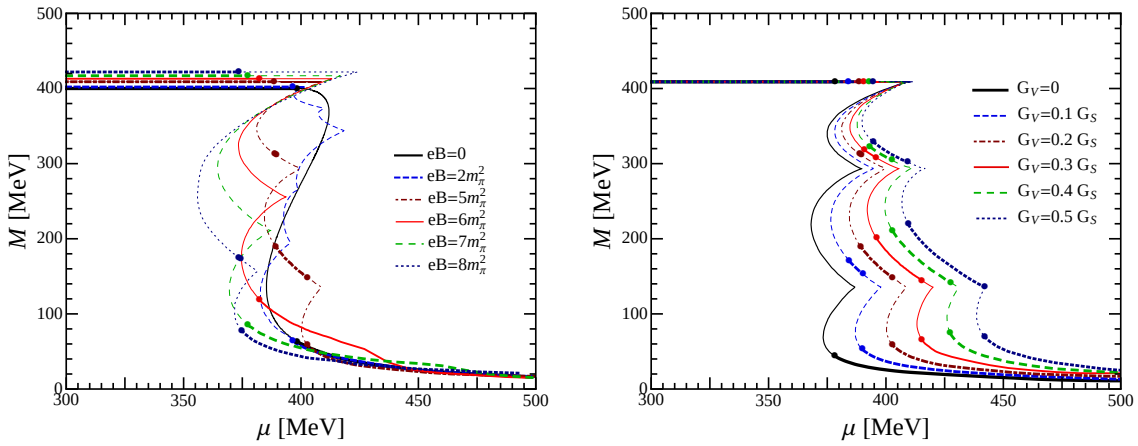

FIG. 1: Cascade of first order transitions. Left panel: The effective quark mass, M, at $T = 0$, as a function of μ for different values of eB at $G_V = 0.2\,G_S$. Right panel: The effective quark mass, M, at $T = 0$, as a function of μ for different values of G_V at $eB = 5\,m_\pi^2$. In both cases the thick lines represent stable solutions to the gap equation.

$M = 190\,\text{MeV}$ at $\mu = 390\,\text{MeV}$. To complete the "cascade" of (three) first order phase transitions one observes a final transition from $M = 150\,\text{MeV}$ to $59\,\text{MeV}$ at $\mu = 402.65\,\text{MeV}$. The numerical results illustrated by the figure clearly display the effective mass oscillatory behavior showing that at relatively weak magnetic fields we observe many oscillations of quark mass values (due to the many Landau levels available). When the field becomes stronger, the quantity of oscillations in the quark effective mass is reduced since there are less Landau levels available. The left panel also shows that, for a fixed value of G_V, the transition to the chiral phase (lowest mass value) occurs at lower chemical potential coexistence values as B increases in accordance with the IMC phenomenon. The right panel shows that, for a fixed B, the transition to the chiral phase occurs at higher chemical potential coexistence values as G_V increases (for a complete discussion on these issues the reader is referred to Ref. [18]). For our present purposes it is important to note how the insertion of a repulsive vector coupling G_V between quarks brings stability ($dM/d\mu \leq 0$) to the system and occasionally promotes these magnetic intermediary density states to stable ones as the right panel shows.

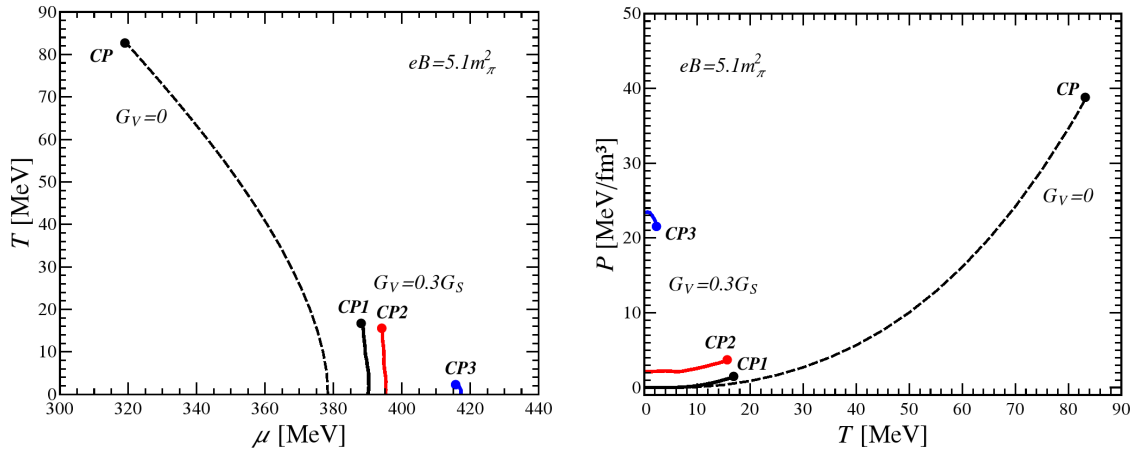

FIG. 2: Quark matter phase diagrams in the $T-\mu$ plane (left panel) and in the $P-T$ plane (right panel) for $eB = 5.1\,m_\pi^2$ and $G_V = 0.3\,G_S$. In both figures the continuous thin line represents the case with $G_V = 0$ for comparison. When $G_V = 0.3\,G_S$ a cascade of three first order transitions appear at very low temperatures. Each first order transition line terminates at the indicated critical point.

Figure 2 shows the $T-\mu$ and $P-T$ phase diagrams for the case of a field strength[3] $eB = 5.1\, m_\pi^2$ and a vector coupling magnitude of $G_V = 0.3\, G_S$, which is the value recently suggested by Sugano et al. [36], compared to the $G_V = 0$ case. At temperatures close to zero, one observes a splitting of the $G_V = 0$ first order transition line into three lines occurring at different μ values as one could expect from the discussion related to figure 1. As already emphasized this exotic scenario may also appear in the $G_V = 0$ case provided that one uses a different parametrization for G_S as discussed in Refs. [20–22]. Here, we have instead adopted a rather canonical value for G_S so that only one transition occurs if $G_V = 0$. This standard choice is well suited to achieve our goal since the role played by the vector channel itself can be further highlighted. The left panel of this figure shows that, as expected [39], G_V weakens the first order transition and shifts the coexistence chemical potential to high values. Note also that for $G_V \neq 0$ the third transition (thick continuous line) is quickly washed out for temperatures higher than $\approx 4.75\,\mathrm{MeV}$. The right panel shows the phase diagram in the physically more intuitive $P-T$ plane. It is interesting to note that the transition terminating at CP3, which is associated with the Landau level jump $k_d = 1 \to 2$, has a negative $\Delta P/\Delta T$ slope (related the Clausius-Clayperon equation) while the ones terminating at $CP1$ and $CP2$, associated with $k_d = 0 \to 0$, have a positive slope just like the one usually observed when $G_V = 0$. Therefore, apart from the usual "liquid-gas" type of transition (positive slope) it appears that the combined presence of G_V and B may also induce a transition of the "solid-liquid" type observed in the water phase diagram (negative slope) which, as far as we know, has not been observed before within QCD motivated models.

Next, in the left panel of Fig. 3 we show the phase diagram in the $T-\rho_B$ plane which could not be analyzed in the previous applications at $T = 0$ [20–22, 38]. The figure shows that for the chosen G_V and B a values a shrinkage of the coexistence regions also takes place. At $T = 0$ the figure shows a coexistence between the following pairs of densities: $\rho_B = 0$ and $\rho_B = 0.8\,\rho_0$ (at $\mu = 388.55\,\mathrm{MeV}$); $\rho_B = 0.9\,\rho_0$ and $\rho_B = 1.7\,\rho_0$ (at $\mu = 390\,\mathrm{MeV}$); and $\rho_B = 2\,\rho_0$ and $\rho_B = 2.55\,\rho_0$ (at $\mu = 402.65\,\mathrm{MeV}$) whereas for the $G_V = 0$ case the dilute phase occurs at vanishing density and the dense phase occurs at $\rho_B = 3\,\rho_0$. As usual the baryonic density is defined as $\rho_B = \rho/3$ while $\rho_0 = 0.17\,\mathrm{fm}^{-3}$. According to Refs [19, 40] one can then expect that the surface tension between the coexistence phases will be lower when $G_V \neq 0$. The right panel of Fig. 3 shows a three dimensional plot displaying the $P-T-\rho_B$ phase diagram with the Andrews isotherms that define the equation of state. This figure indicates that the cascade of three first order transition observed so far always refer to the coexistence of two phases occurring at distinct pressures.

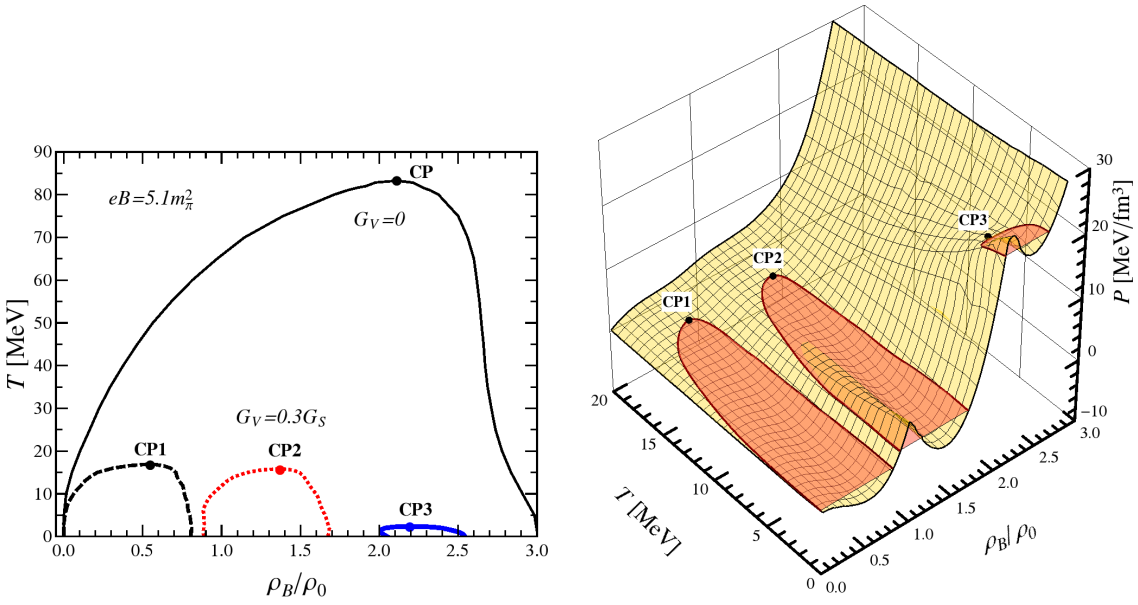

FIG. 3: Left Panel: Coexistence phase diagram in the $T-\rho_B$ plane for $eB = 5.1\, m_\pi^2$ and $G_V = 0.3\, G_S$. The case $G_V = 0$ (thin continuous line) is shown for comparison. Right panel: The phase diagram in the $P-T-\rho_B$ space. In both panels it is possible to distinguish the three independent first order phase transitions defined by the coexistence of two distinct densities at the same pressure.

Up to this point we have seen that, due to the LL filling procedure, chiral symmetry restoration may take place via

[3] The choice of this particular value will become clear in the sequel.

successive first order transitions between different magnetized phases. From the free energy perspective this succession happens because, depending on the values of the couplings, the presence of a magnetic field may induce the appearance of more than two minima so that by varying a control parameter, such as μ, one may observe multiple transitions. This scenario can happen either when $G_V = 0$ and G_S is relatively weak (leading to effective quark masses such as $M \approx 200\,\mathrm{MeV}$) [20–22] or when $G_V \neq 0$ but G_S leads to more standard M values as we have shown. At this point it is crucial to note that, with the values of G_V and B considered so far, we have only observed the occurrence of two degenerate global minima signaling the usual type of first order phase phase transition for a given value of μ while any eventual extra minima remain local. Then, at another chemical potential value a global minimum turns into a local one and vice versa leading us to observe a cascade of transitions where only two densities coexist for a given value of μ. The results found in this section suggest that perhaps there are certain values of G_V at which three degenerate global minima will emerge signaling the coexistence of *three* different phases at the same T, μ and B values as we shall discuss next.

IV. FIRST ORDER CHIRAL TRANSITIONS WITH THREE COEXISTING DENSITIES

The previous discussion shows that the B and G_V values considered so far produce a cascade of first order transitions where, at a given coexistence μ value, only a pair of degenerate (global) minima coexist with other (local) minima. However, for other parameter values, it may be energetically preferable that one of these local minima becomes a global one so that the ground state is triply degenerated. With this motivation let us now scan G_V and eB around the values $G_V = 0.2\,G_S$ and $eB = 5\,m_\pi^2$. Fig. 4 shows the thermodynamic potential evaluated at $eB = 5.1\,m_\pi^2$ and $G_V = 0.2\,G_S$ at various temperatures. To facilitate the understanding of the unusual phase diagrams which appear in the sequel let us discuss the results shown in this figure with some detail. Starting with the $T = 0$ case one observes (left panel) three coincident minima occurring at the same null pressure coexistence chemical potential value $\mu_{TP1} = 388.05\,\mathrm{MeV}$ where the subscript stands for "triple point 1".

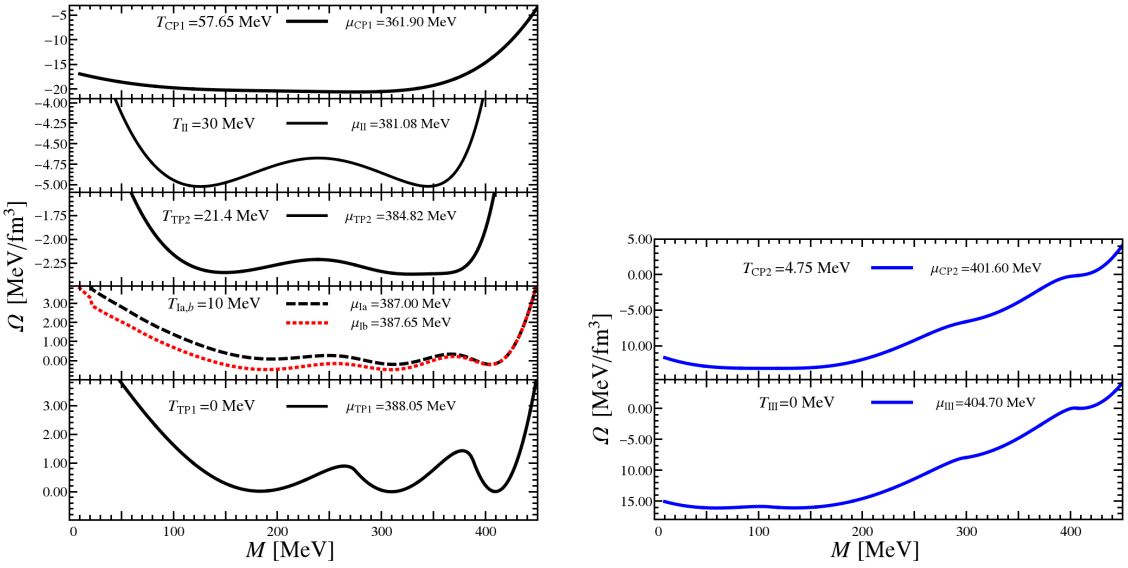

FIG. 4: Thermodynamic potential at $G_V = 0.2\,G_S$ and $eB = 5.1\,m_\pi^2$ for some selected temperatures. Left panel: at $T = 0$ the potential is triply degenerate at the coexistence chemical potential value $\mu_{TP1} = 388.05\,\mathrm{MeV}$. At $T = 10\,\mathrm{MeV}$ the potential is doubly degenerate at two different coexistence chemical potential values, $\mu_{Ia} = 387\,\mathrm{MeV}$ and $\mu_{Ib} = 387.65\,\mathrm{MeV}$. At $T = 21.4\,\mathrm{MeV}$ it becomes triply degenerate again, at $\mu_{TP2} = 384.82\,\mathrm{MeV}$ while at $T = 30\,\mathrm{MeV}$ it is doubly degenerate at $\mu_{II} = 381.08\,\mathrm{MeV}$. Right panel:

At $T = 10\,\mathrm{MeV}$ this triple coexistence at the same chemical potential no longer survives and one observes the dissociation into two separate first order transitions occurring at two distinct coexistence chemical potential values $\mu_{Ia} = 387\,\mathrm{MeV}$ and $\mu_{Ib} = 387.65\,\mathrm{MeV}$, respectively which signals a "cascade" of two subsequent first order phase transitions. At a higher temperature, near $T_{TP2} = 21.4\,\mathrm{MeV}$, three degenerate minima are again observed and one can ascribe another triple point taking place at $\mu_{TP2} = 384.82\,\mathrm{MeV}$. Above this temperature, we observe the usual behavior of the chiral with only one first order transition which evolves to the critical point as T increases. The right

panel of Fig. 4 shows a final transition line starting at $T = 0$ and $\mu_{III} = 404.70\,\mathrm{MeV}$ and terminating at the CP located at $T_{CP2} = 4.75\,\mathrm{MeV}$ and $\mu_{CP2} = 401.60\,\mathrm{MeV}$.

Notice that in the previous section we have deliberately shown results for the cases $G_V = 0.2\,\mathrm{MeV}$ and $eB = 5\,\mathrm{MeV}$ as well as for $G_V = 0.3\,\mathrm{MeV}$ and $eB = 5.1\,\mathrm{MeV}$ but not for the present choice, $G_V = 0.2\,\mathrm{MeV}$ and $eB = 5.1\,\mathrm{MeV}$, which induces the appearence of triple points. As already discussed the quark effective mass is directly related to the order parameter so that the discussion can be further clarified by investigating how this quantity varies with μ for the T, G_V and B values considered in Fig. 4. With this aim we present Fig. 5 where one may observe the transitions discussed in connection with the former figure from a different perspective. The squares locate the first triple point, the triangles locate the second triple point while the ordinary type of first order transitions is denoted by the dots.

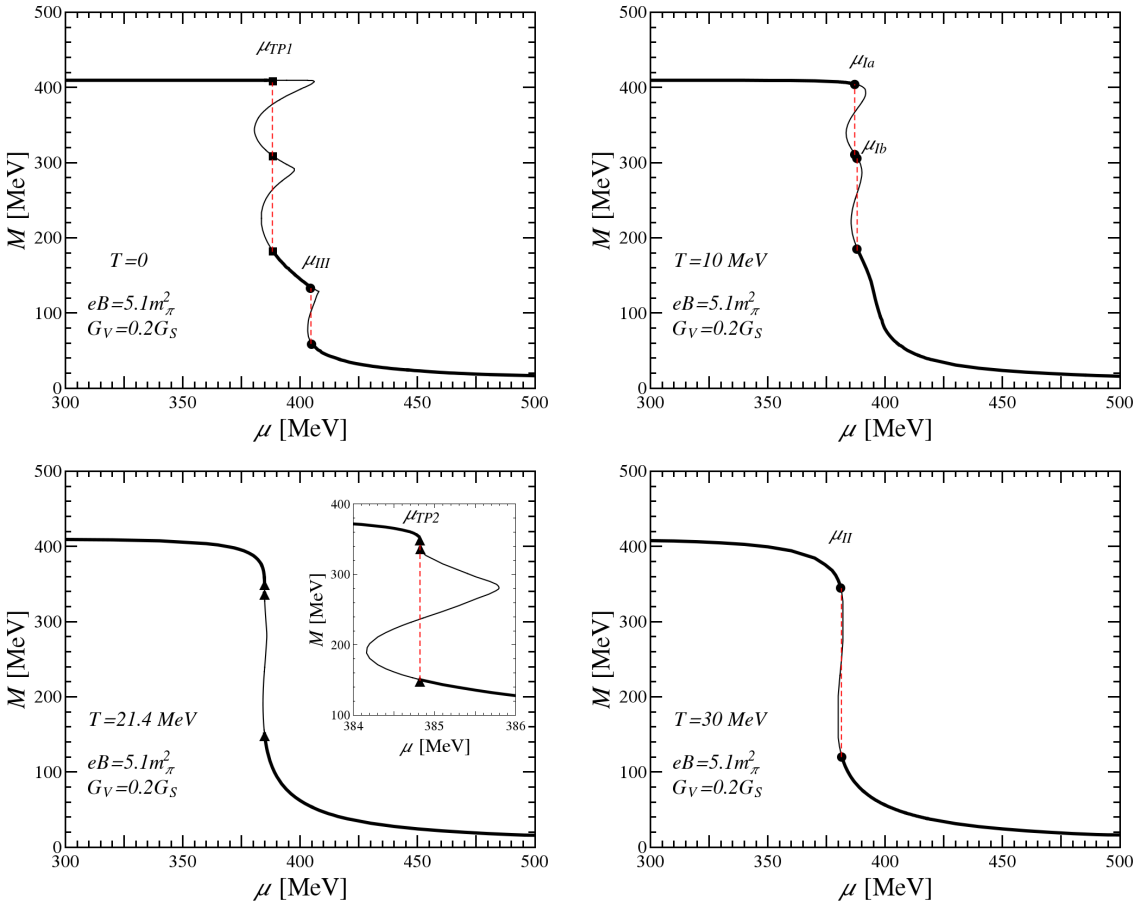

FIG. 5: Sequence of plots showing first order chiral transitions for $eB = 5.1\,m_\pi^2$ and $G_V = 0.2\,G_S$. The squares and triangles indicate triply degenerate transitions while the dots indicate doubly degenerate ones.

From the sequence shown, it becomes evident how the triple point $TP1$, related to three different mass values (marked by the squares), determines the same chemical potential $\mu_{TP1} = 388.05\,\mathrm{MeV}$ when $T = 0$. Note that the the three mass values, satisfying the gap equation, differ by an approximately equal amount (close to 100 MeV). Still at $T = 0$ but at a higher chemical potential value one observes the occurrence of another (ordinary) transition signaled by two different mass values (marked by the dots) at $\mu_{III} = 404.70\,\mathrm{MeV}$. Then, rising the temperature to $T = 10\,\mathrm{MeV}$ one sees that the triple coexistence, observed at $T = 0$, decouples into two ordinary first order transitions occurring at two different, but yet very similar, chemical potentials given by $\mu_{Ia} = 387\,\mathrm{MeV}$ and $\mu_{Ib} = 387.65\,\mathrm{MeV}$. At this temperature the first order line starting at μ_{III} and $T = 0$ has already vanished. Note also that the low mass value occurring at μ_{Ia} and the high mass value occurring μ_{Ib} are almost identical (the difference amounts to about 5 MeV). Near $T = 21.4\,\mathrm{MeV}$, these distinct first order lines start to approach each other and one observes another triple point ($TP2$) at μ_{TP2} marked by the triangles. In this case the high and the intermediate mass values become almost identical but differ substantially from the low value (by almost 200 MeV). Above this temperature, as the $T = 30\,\mathrm{MeV}$ panel suggests, only the ordinary scenario takes place until the first order transition line ends at a critical point, $CP1$, located at $T_{CP1} = 57.65\,\mathrm{MeV}$ and $\mu_{CP1} = 361.90\,\mathrm{MeV}$.

We are now in position to map all these transitions into phase diagrams such as the ones shown in Fig. 6 in order to display the phase boundaries in the $T-\mu$ and $P-T$ planes.

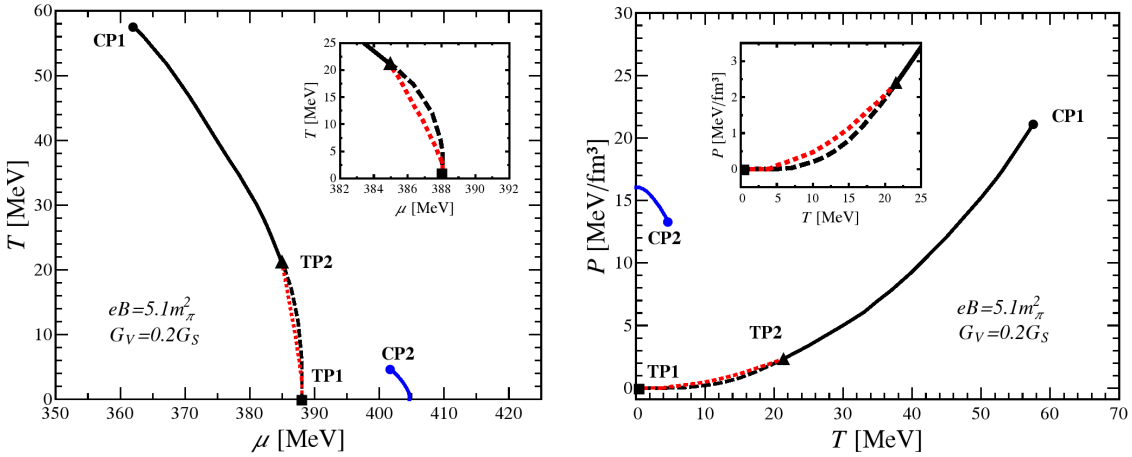

FIG. 6: Phase diagrams in the $T-\mu$ plane (Left Panel) and in the $P-T$ plane (Right Panel) for$B=5.1\,m_\pi^2$ and $G_V=0.2\,G_S$. At $T=0$, both diagrams show a triple point (TP1) splits into two common dual-phase coexistence lines as the zoomed areas show. At $T_{TP2}=21.4\,\mathrm{MeV}$, the dual coexistence lines converge again and merge at another triple point (TP2). Beyond this temperature one observes the ordinary first order line which ends in a critical point (CP1). The figure also shows that the first order phase transition line which terminates at CP2 has a negative $\Delta P/\Delta T$ slope.

Analyzing these figures we verify that the usual phase diagrams are drastically modified from the ordinary case at $G_V=0$ since we now have a first-order coexistence line originating from a triple point at $(T=0,\mu_{TP1}=388.05\,\mathrm{MeV})$ and then splitting into two new branches of ordinary first order transitions, as shown in the zoomed region, to finally merge again at a second triple point $(T_{TP2}=21.4\,\mathrm{MeV},\mu_{TP2}=384.82\,\mathrm{MeV})$. Then, for higher temperatures the transition always follows the usual pattern until the line ends a critical point (CP1). The figure also shows an ordinary first order phase transition line which starting at $(T=0,\mu_{III}=404.70\,\mathrm{MeV})$ and terminating at CP2 $(T_{CP2}=4.75\,\mathrm{MeV},\ \mu_{CP2}=401.60\,\mathrm{MeV})$. The $P-T$ allows to further understand these two different first order lines by observing the dP/dT slope in each case. The diagram shows that the line terminating at CP1 has a positive slope just like in the well known "liquid-gas" type of transition while the line terminating at CP2 presents a negative slope which is reminiscent of the "solid-liquid" transition occuring in the water phase diagram which does not appear to have been reported previously (at least within the context of strongly interacting systems). The left panel of Fig. 7 displays the coexistence phase diagram in the $T-\rho_B$ plane while the right panel of the same figure shows a three dimensional plot displaying the $P-T-\rho_B$ phase diagram with the Andrews isotherms.

It is well known that at zero temperature this type of model, as well as the quark meson model, typically predict phase coexistence between the vacuum and the dense quark phase, similar to the "liquid-gas" transition. However, we now observe that when a vector repulsion and a magnetic field are present it is possible that three phases coexist for particular parameter values. As Fig. 7 shows, for $eB=5.1\,,m_\pi^2$ and $G_V=0.2\,G_S$, one observes the coexistence between phases with densities $\rho_B/\rho_0=0,0.85\,,\mathrm{and}\,1.75$ which is a rather interesting result since the vanishing density represents the vacuum, the intermediate density value is very close to that of ordinary nuclear matter while the third is close to the values this model predicts for the dense quark phase. Eventually, by scanning over parameter values one may force the intermediate density to take place at $\rho_B/\rho_0=1$ so that this could be identified as nuclear matter. As the temperature increases, the three-phase coexistence vanishes and one observes a decoupling into two separate branches Ia and Ib, which are related to two first order transitions taking place at distinct pressure values. This bifurcation in two coexistence branches creates a stability island between the regions Ia and Ib. Again, at $T_{TP2}=21.4\,\mathrm{MeV}$ these two distinct first order transitions will share the same pressure at a triple point $TP2$ as the figures show. The remaining first order transition corresponding to the coexistence region II ends at an ordinary critical point $CP1$. Furthermore, as already emphasized, another coexistence region appears at a higher density range, labelled as III in the left panel of Fig. 7. At $T=0$ the coxistence densities for this region are $\rho_B/\rho_0=2.0$ and $\rho_B/\rho_0=2.6$. Then, when the temperature reaches the critical value $T_{CP2}=4.75\,\mathrm{MeV}$ this coexistence region, which corresponds to a "solid-liquid" type of transition, terminates at $CP2$.

At this point it is important to recall that the occurrence of multiple phases at the same pressure is only possible if thermodynamical potential develops multiple global minima. This condition can be attained to a particular choice of B and G_V values which give rise to multiple densities coexisting in the same transition chemical potential μ. Let us

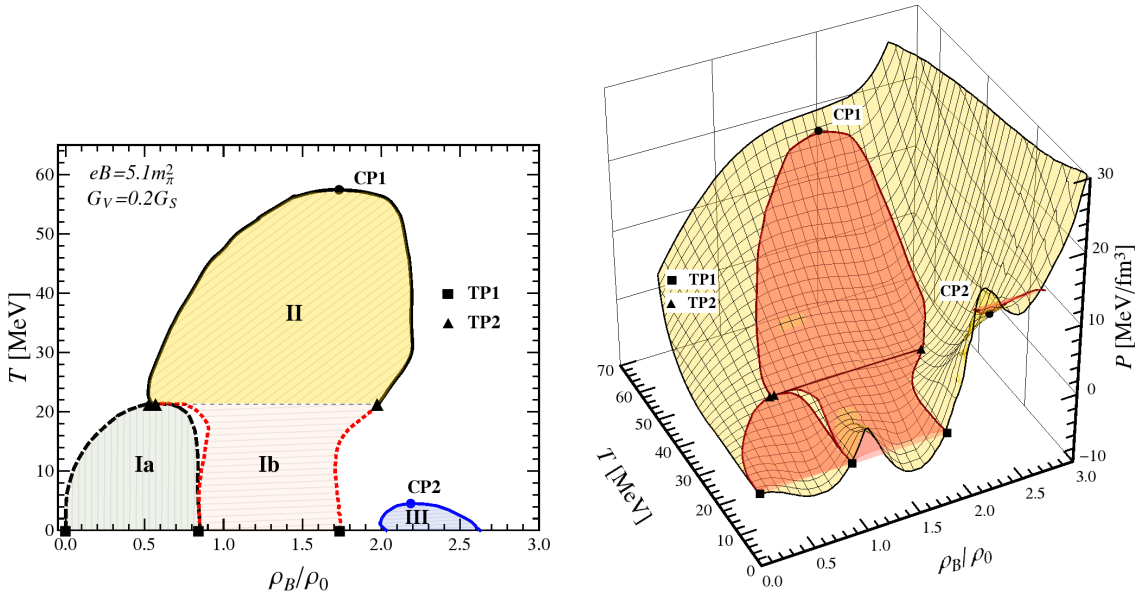

FIG. 7: Phase diagram in the $T-\rho_B$ plane (Left Panel) and EOS isotherms in the $P-T-\rho_B$ space (Right Panel) for the $B=5.1\,m_\pi^2$ and $G_V=0.2\,G_S$ case. Filled squares and triangles indicate the triple points and filled circles indicate the critical end points in accordance with the previous figures.

now call G_V^c the critical vector coupling value at which three degenerate global minima appear for a given B value. Then, when mapping the parameter space of (B, G_V^c, μ) values which result in a three-phase coexistence at $T=0$ we encounter the oscillatory behavior shown in Fig. 8.

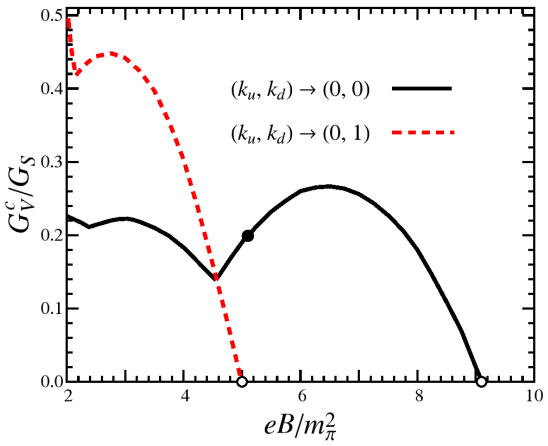

FIG. 8: Magnetic field dependence of the critical values, G_V^c, related to the transitions $(k_u,\,k_d)\to(0,0)$ and $(k_u,\,k_d)\to(0,1)$ at $T=0$. The dot labels the values used in our analyzes and the open circles mark the excluded $G_V=0$ case.

Each critical vector coupling G_V^c can be associated with the emergence of a new intermediary (stable) value of the order parameter. Depending on the field strength, more than one intermediary Landau level configuration $(k_u,\,k_d)$ can appear and each one has its own G_V^c value. So, it must exist an infinite set of critical values G_V^c associated with the infinite number of intermediary states $(k_u,\,k_d)$ in the limit of $B\to 0$ and $G_V\to\infty$. The figure only shows the first two possibilities characterized by the transitions $(k_u,\,k_d)\to(0,0)$ and $(k_u,\,k_d)\to(0,1)$. As one can observe the former transition covers the region of the parameter values which are usually considered in the recent literature ($G_V=0-0.5\,G_S$ and $eB=2-8\,m_\pi^2$). Note that for high fields $eB\gtrsim 9\,m_\pi^2$ the emergence of triple points is suppressed since only the LLL is occupied. We have tested coupling values above and below the critical line observing that when $G_V<G_V^c$ only the traditional case with one first order transition line emerges. Then, when $G_V=G_V^c$ the multiple coexistence becomes possible and a new first order transition lines starts from the original one at $T=0$ as shown

in Figs. 6 and 7. Finally, when $G_V > G_V^c$ the chiral symmetry restoration takes place via more than one first order transition line in a cascade mode as discussed in Section III. We close this section by remarking that we have also observed the coexistence of four phases but this is resctrited to the $T = 0$ case only.

V. CONCLUSIONS

We have investigated how the presence of a magnetic field and a repulsive vector interaction may influence the phase diagram of strongly interacting matter generating unusual transition patterns associated to first order chiral transitions. In the first part of the present study we have considered parameter values which produce a cascade of first order transitions similar to the ones analyzed in Refs. [20–22] at vanishing temperatures. We have taken a step forward by incorporating the vector interaction as well as by pushing the evaluations to the finite temperature domain in order to better understand the physical nature of such transitions. Mapping the transition into the $P - T$ plane has allowed us to observe that the transition which takes place at high pressure has a negative dP/dT slope which is reminiscent of the "solid-liquid" transition observed in the water phase diagram while the remaining (low pressure) transitions have a positive slope and therefore resemble the "liquid-gas" transition which is usually observed within effective quark models. Having in mind that, due to the inherent oscillations caused by the filling of Landau levels, the magnetic field induces the free energy to develop multiple minima while the repulsive vector interaction favors stability we have scanned over B and G_V values to check for the possibility of observing three degenerate global minima which would then lead to the existence of a triple point. Our expectation was confirmed by the numerical investigation and we were able to find, for a given value of B, a certain value of G_V so that three (instead of the usual two) phases coexist which, as far as we know, has not been observed before. In contrast to the "solid-liquid" type of transition, which may be find when canonical parametrizations are used, the existence of triple points is only possible when very specific values of G_V are chosen. Finally, we point out remark that the coexistence of multiple phases has also been recently observed by Manso and Ramos [41] within the $2 + 1$ d Gross-Neveu model despite the fact that a repulsive term has not been considered. Instead the authors have considered a tilted magnetic field observing that the parallel component tends to stabilize the free energy (just as G_V in our case) so that three degenerate minima were also observed. Together with our observations this result leads us to conclude that the phase diagram of magnetized matter may display the coexistence of multiple phases if the dynamics contains terms which bring stability to the free energy.

Acknowledgments

This work was partially supported by Conselho Nacional de Desenvolvimento Científico e Tecnológico (CNPq).

[1] K. Fukushima, D. E. Kharzeev and H. J. Warringa, Phys. Rev. D **78** 074033 (2008); D. E. Kharzeev and H. J. Warringa, Phys. Rev. D **80** 034028 (2009); D. E. Kharzeev, Nucl. Phys. A **830**, 543c (2009).
[2] R. Duncan and C. Thompson, Astron. J, **32**, L9 (1992); C. Kouveliotou et al., Nature **393**, 235 (1998).
[3] K. Tuchin, Adv. High Energy Phys. **2013**, 490495 (2013); Phys. Rev. C **88**, 024911 (2013).
[4] L. McLerran and V. Skokov, Nucl. Phys. A **929**, 184 (2014).
[5] S. P. Klevansky and R. H. Lemmer, Phys. Rev. D **39**, 3478 (1989); H. Suganuma and T. Tatsumi, Annals Phys. **208**, 470 (1991); K.G. Klimenko, Theor. Math. Phys. 89 , 1161 (1992); Z. Phys. C 54, 323 (1992); K.G. Klimenko, A.S. Vshivtsev, and B.V. Magnitsky, Nuovo Cimento A107, 439 (1994); V.P. Gusynin, V.A. Miransky, and I.A. Shovkovy, Phys. Rev. Lett. 73, 3499 (1994).
[6] I. A. Shovkovy, Lect. Notes Phys. **871**, 13 (2013).
[7] E. S. Fraga, arXiv:1310.6656 [hep-ph]; J. O. Andersen, W. R. Naylor and A. Tranberg, arXiv:1411.7176 [hep-ph]; V. A. Miransky and I. A. Shovkovy, arXiv:1503.00732 [hep-ph].
[8] A.J. Mizher, M.N.Chernoub and E.S. Fraga, Phys. Rev. D **82** 105016 (2010).
[9] S.S. Avancini, D.P. Menezes, M.B. Pinto and C. Providência, Phys. Rev. D **85**, 091901 (2012).
[10] J. O. Andersen and A. Tranberg, JHEP **1208**, 002 (2012).
[11] A.F. Garcia, G.N. Ferrari and M.B. Pinto, Phys. Rev. D **86**, 096005 (2012).
[12] M. D'Elia, S. Mukherjee and F. Sanfilippo, Phys. Rev. D **82**, 051501 (2010).
[13] G. S. Bali, F. Bruckmann, G. Endrodi, Z. Fodor, S. D. Katz, S. Krieg, A. Schafer and K. K. Szabo, JHEP **1202**, 044 (2012); G. S. Bali, F. Bruckmann, G. Endrodi, Z. Fodor, S. D. Katz and A. Schafer, Phys. Rev. D **86**, 071502 (2012).
[14] Y. Aoki, G. Endrodi, Z. Fodor, S.D. Katz and K.K. Szabo, Nature **443**, 675 (2006); Y. Aoki, Z. Fodor, S.D. Katz and K.K. Szabo, Phys. Lett. B **643**, 46 (2006).

[15] M. Ferreira, P. Costa, D.P. Menezes, C. Providência and N. Scoccola, Phys. Rev. D **89**, 016002 (2014); M. Ferreira, P. Costa, O. Lourenço, T. Frederico, and C. Providência Phys. Rev. D **89**, 116011 (2014); R. L. S. Farias, K. P. Gomes, G. I. Krein and M. B. Pinto, Phys. Rev. C **90**, 025203 (2014).
[16] F. Preis, A. Rebhan and A. Schmitt, JHEP **1103**, 033 (2011).
[17] F. Preis, A. Rebhan and A. Schmitt, Lect. Notes Phys. **871**, 51 (2013).
[18] R. Z. Denke and M. B. Pinto, Phys. Rev. D **88** 056008 (2013).
[19] A.F. Garcia and M.B. Pinto, Phys. Rev. C **88** 025207 (2013).
[20] D. Ebert, K.G. Klimenko, M.A. Vdvichenko and A.S. Vshivtsev, Phys. Rev. D **61**, 025005 (1999); A.S. Vshivtsev and K.G. Klimenko, JETP Lett. **64** 338 (1996); K.G. Klimenko, arXiv: hep-ph/9809218 (1998).
[21] P.G. Allen and N.N.Scoccola, Phys. Rev. D **88** 094005 (2013).
[22] A.G. Grunfeld, D.P. Menezes, M.B. Pinto, M.B. and N.N. Scoccola, Phys. Rev. D **90** 044024 (2014).
[23] J.-L. Kneur, M.B. Pinto and R.O. Ramos, Phys. Rev. D **88**, 045005 (2013).
[24] J.D. Walecka and B.D. Serot, Adv. Nucl. Phys. **16**, 1 (1986).
[25] V. Koch, T. S. Biro, J. Kunz, and U. Mosel, Phys. Lett. B **185**, 1 (1987).
[26] D. P. Menezes, M. B. Pinto, L. Castro, P. Costa and C. Providência, Phys. Rev. C **89** 055207 (2014).
[27] Y. Nambu and G. Jona-Lasinio, Phys. Rev. **122**, 345 (1961); *ibid.* **124**, 246 (1961).
[28] M. Buballa, Phys. Rep. **407**, 205 (2005).
[29] E.S. Fraga and A.J. Mizher, Phys. Rev. D**78**, 025016 (2008).
[30] D.P. Menezes, M.B. Pinto, S.S. Avancini, A. Pérez Martínez and C. Providência, Phys. Rev. **C 79**, 035807 (2009).
[31] J. Noronha and I. A. Shovkovy, Phys. Rev. **D 76**, 105030 (2007).
[32] K. Fukushima and H.J. Warringa, Phys. Rev. Lett. **100**, 032007 (2008).
[33] D. Ebert, K.G. Klimenko, M.A. Vdovichenko and A.S. Vshivtsev, Phys. Rev. D **61**, 025005 (1999).
[34] R. Rapp, T. Schafer and E.V. Shuryak, Phys. Rev. Lett. **81**, 53 (1998).
[35] C. Carignano, D. Nickel and M. Buballa, Phys. Rev. D **82**, 054009 (2010).
[36] J. Sugano, J. Takahashi, M. Ishii, H. Kouno and M. Yahiro, Phys. Rev. D **90**, 037901 (2014).
[37] J. -L. Kneur, M. B. Pinto and R. O. Ramos, Phys. Rev. C **81**, 065205 (2010); L. Ferroni, V. Koch and M.B. Pinto, Phys. Rev. C **82**, 055205 (2010); T. E. Restrepo, J. C. Macias, M. B. Pinto and G. N. Ferrari, Phys. Rev. D **91**, no. 6, 065017 (2015).
[38] P.G. Allen, V.P. Pagura and N.N. Scoccola, arXiv: hep-ph/1502.00572 (2015).
[39] K. Fukushima, Phys. Rev. D **78**, 114019 (2008).
[40] J. Randrup, Phys. Rev. C **79**, 054911 (2009).
[41] R.O. Ramos and P.H.A. Manso, Phys. Rev. D **87**, 125014 (2013).